JOURNAL OF GEOPHYSICAL RESEARCH, VOL. 109, B01303, DOI:10.1029/2003JB002497,

Temperature fields generated by the elastodynamic propagation of shear cracks in the Earth

Yuri Fialko

Institute of Geophysics and Planetary Physics, Scripps Institution of Oceanography, University of California San Diego, La Jolla, California

Abstract.

Thermal perturbations associated with seismic slip on faults may significantly affect the dynamic friction and the mechanical energy release during earthquakes. This paper investigates details of the co-seismic temperature increases associated with the elastodynamic propagation of shear cracks, and effects of fault heating on the dynamic fault strength. Self-similar solutions are presented for the temperature evolution on a surface of a Mode II shear crack and a self-healing pulse rupturing at a constant velocity. The along-crack temperature distribution is controlled by a single parameter, the ratio of the crack thickness to the width of the conductive thermal boundary layer, $\bar{w}$. For "thick" cracks, or at early stages of rupture ($\bar{w} > 1$), the local temperature on the crack surface is directly proportional to the amount of slip. For "thin" cracks, or at later times ($\bar{w} < 1$), the temperature maximum shifts toward the crack tip. For faults having slip zone thickness of the order of centimeters or less, the onset of thermally-induced phenomena (e.g., frictional melting, thermal pressurization, etc.) may occur at any point along the rupture, depending on the degree of slip localization, and rupture duration. In the absence of significant increases in the pore fluid pressure, localized fault slip may raise temperature by several hundred degrees, sufficient to cause melting. The onset of frictional melting may give rise to substantial increases in the effective fault strength due to an increase in the effective fault contact area, and high viscosity of silicate melts near solidus. The inferred transient increases in the dynamic friction ("viscous braking") are consistent with results of high-speed rock sliding experiments, and might explain field observations of the fault wall rip-out structures associated with pseudotachylites. Possible effects of viscous braking on the earthquake rupture dynamics include 1) de-localization of slip and increases in the effective fracture energy, 2) transition from a crack-like to a pulse-like rupture propagation, or 3) ultimate rupture arrest. Assuming that the pulse-like ruptures heal by incipient fusion, the seismologic observations can be used to place a lower bound on the dynamic fault friction. This bound is found to be of the order of several megapascals, essentially independent of the earthquake size. Further experimental and theoretical studies of melt rheology at high strain rates are needed to quantify the effects of melting on the dynamic fault strength.

1. Introduction

The efficiency at which earthquakes convert the potential energy of elastically deformed rocks into seismic radiation depends on dissipative losses (e.g., work done against friction) on earthquake faults. Although the amount of energy dissipated during earthquakes is generally unknown, indirect estimates suggest that frictional losses may constitute a significant (if not dominant) part of the earthquake energy budget [e.g., *Kanamori and Anderson*, 1975; *McGarr*, 1980; *Scholz*, 1990, p.165]. Because most of the energy dissipated on a fault is ultimately converted into heat, there is a possibility that the co-seismic increases in temperature may affect the frictional properties of rocks in the fault zone, and the dynamic stress drop during earthquakes [*Sibson*, 1977; *Lachenbruch*, 1980]. Over the last two decades, significant insights into the earthquake dynamics have been obtained using the laboratory-derived rate and state friction models [*Dieterich*, 1992; *Ruina*, 1983; *Tse and Rice*, 1986]. While the rate and state friction may adequately describe the nucleation and initial rupture phases of seismic instabilities, theoretical arguments [e.g., *McKenzie and Brune*, 1972; *Cardwell et al.*, 1978], field observations [*Price*, 1970; *Sibson*, 1975; *Swanson*, 1992], and experimental data [*Spray*, 1993; *Tsutsumi and Shimamoto*, 1997; *Goldsby and Tullis*, 2002] indicate that the co-seismic temperature increases may dramatically modify the constitutive behavior of the fault zone rocks at seismic slip rates of the order of 1 m/s. A better understanding of interactions between the frictional heating and the dynamic fault strength requires a detailed knowledge of spatiotemporal variations in temperature that lead to the onset of the thermally-induced variations in friction. In this paper I investigate thermal evolution of two-dimensional (2-D) elastodynamic ruptures having a finite thickness of a slip zone, and propagating at a finite velocity. In particular, I address the question of where on the slipping fault the onset of the thermally-induced weakening (or strengthening) is likely to occur. Implications from theoretical results are then discussed in the light of available experimental and field data relevant to the dynamics of seismic slip.

0148-0227/05/2003JB002497$9.00

2. Spatiotemporal evolution of temperature on a fault plane

Thermal aspects of seismic faulting were considered by a number of studies. *Jeffreys* [1942] obtained dimensional estimates for the co-seismic temperature increases on a fault slipping at a constant velocity, assuming that the fault is infinitesimally thin, and the frictional heat production is balanced by the conductive heat loss to the surrounding rocks. He found that temperature increases of the order of 10^3 K (i.e., sufficient to cause melting) should occur after only a few centimeters of slip at 1 km depth. *McKenzie and Brune* [1972] obtained one-dimensional time-dependent solutions for the Jeffrey's problem, and *Cardwell et al.* [1978] extended the results of *McKenzie and Brune* [1972] to a case of a finite thickness of the slip zone. Solutions of *Jeffreys* [1942]; *McKenzie and Brune* [1972] and *Cardwell et al.* [1978] all assume a constant slip velocity (or, equivalently, an infinite rupture velocity, or an infinite fault size). Such an assumption is invalid for the elastodynamic shear instabilities characterized by significant along-rupture variations in particle velocities [*Scholz*, 1990; *Freund*, 1998]. *Richards* [1976] presented double integral expressions for a temperature distribution on a surface of an infinitesimally thin circular shear crack expanding at a constant velocity. However, he did not evaluate his results numerically, and such an evaluation appears to be difficult (P. Richards, personal communication, 2000). *Lee and Delaney* [1987] and *Andrews* [2002] have considered temperature increases near the leading edge of a propagating crack in the context of thermal pressurization of pore fluids.

Dimensionally, the temperature increase ΔT due to fault slip D may be obtained by balancing the work against friction, $\sigma_f D$, and the conductive heat loss to the ambient rocks, $2wc\rho\Delta T$ [e.g., *Cardwell et al.*, 1978],

$$\Delta T = \frac{\sigma_f D}{2wc\rho}, \tag{1}$$

where σ_f is the shear stress acting on a fault, c and ρ are the heat capacity and density of the host rock, respectively, and $2w$ is the thickness of the slip zone (gouge layer), or the width of the conductive thermal boundary layer, whichever is larger. For infinitesimally thin shear cracks, the width of the thermal boundary layer is $w_c = \sqrt{2\kappa t_s}$, where κ is the thermal diffusivity of the host rocks, and t_s is the duration of slip. Note that in case of fluid-assisted heat removal from the fault surface (e.g., due to thermal pressurization), the effective width of the thermal boundary layer may be significantly larger than the width of the conductive boundary layer w_c. More detailed predictions of the temperature increase accounting for the along-fault variations in slip velocity, and the non-steady heat transfer require numerical experiments. I start by considering the time-dependent thermal evolution of a two-dimensional shear crack.

2.1. Co-seismic temperature increases due to a crack-like rupture

Consider a Mode II (plain strain) crack rupturing bilaterally at a constant speed V_r (Figure 1). The crack half-length a is zero prior to the rupture initiation, and linearly increases with time after the onset of seismic instability, $a(t) = tV_r$. The host rock temperature T is presumed to obey a 1-D diffusion equation (heat conduction in slip-parallel direction is neglected),

$$\frac{\partial T}{\partial t} = \kappa\frac{\partial^2 T}{\partial y^2} + \frac{Q}{c\rho}, \tag{2}$$

where y is the crack-perpendicular coordinate, and Q is the rate of frictional heat generation within the slipping zone,

$$Q(x,y,t) = \begin{cases} \frac{\sigma_f(x)}{2w(x)}\frac{\partial D(x,t)}{\partial t}, & t>0, |y|<w \\ 0, & |y|>w, \end{cases} \tag{3}$$

where $\partial D/\partial t$ is the local slip velocity. For simplicity, I assume that the thickness of the gouge layer is constant along the crack, and the shear strain rate is uniform across the gouge layer [*Cardwell et al.*, 1978]. Laboratory measurements of the frictionally generated heat indicate that the assumption of a uniform shear within the slip zone may be adequate [*Mair and Marone*, 2000]. A solution to equation (2) subject to the initial condition $T(x,y,0) = T_0$, where T_0 is the temperature of the host rocks prior to faulting, is [e.g., *Morse and Feshbach*, 1953; *Cardwell et al.*, 1978],

$$T(x,y,t) - T_0 = \frac{1}{2c\rho\sqrt{\pi\kappa}}\int_{t_0}^{t}\int_{-\infty}^{\infty}\exp\left[\frac{(y-\zeta)^2}{4\kappa(\tau-t)}\right] \times\frac{Q(x,\zeta,\tau)}{\sqrt{t-\tau}}d\zeta d\tau, \tag{4}$$

where $t_0 = x/V_r$ is the time at which the rupture front passes point x. Substituting equation (3) into (4), and taking the improper inner integral, one obtains

$$T - T_0 = \frac{1}{4c\rho w}\int_{x/V_r}^{t}\left(\mathrm{erf}\left[\frac{y+w}{2\sqrt{\kappa(t-\tau)}}\right] - \mathrm{erf}\left[\frac{y-w}{2\sqrt{\kappa(t-\tau)}}\right]\right)\frac{\partial D(x,\tau)}{\partial\tau}\sigma_f(x)d\tau. \tag{5}$$

Further analytic insights are possible for a case of a self-similar crack propagation. The latter implies that the along-crack displacement profile $D(x,t)$ may be expressed in terms of a single similarity variable $\chi = \chi(x,t)$ (that is, the crack propagates preserving its shape),

$$D(x,t) = a(t)\epsilon D(\chi), \tag{6}$$

where ϵ is the characteristic shear strain due to the crack, $\epsilon = D(0,t)/a(t)$. The strain ϵ is of the order of the ratio of the earthquake stress drop to the shear modulus of the host rocks, and is apparently independent of the earthquake size [*Kanamori and Anderson*, 1975; *Scholz*, 1990; *Abercrombie*, 1995]. Hereafter, ϵ is taken to be constant. It is convenient to introduce similarity variables

$$\text{non-dimensional along-fault coordinate} \quad \chi = \frac{x}{tV_r}, \tag{7}$$

$$\text{non-dimensional fault thickness} \quad \bar{w} = \sqrt{\frac{2}{\kappa t}}w. \tag{8}$$

An expression for the local slip rate in terms of the new variables is obtained by differentiating equation (6),

$$\frac{\partial D}{\partial t} = V_r\epsilon\left[D(\chi) - \chi\frac{\partial D}{\partial\chi}\right]. \tag{9}$$

A dimensional analysis of equations (5) and (9) suggests the following similarity variable for temperature,

$$\text{non-dimensional temperature} \quad \theta = \frac{T-T_0}{\hat{T}}, \tag{10}$$

where

$$\hat{T} = \frac{\sigma_d V_r\epsilon}{c\rho}\sqrt{\frac{t}{\pi\kappa}}, \tag{11}$$

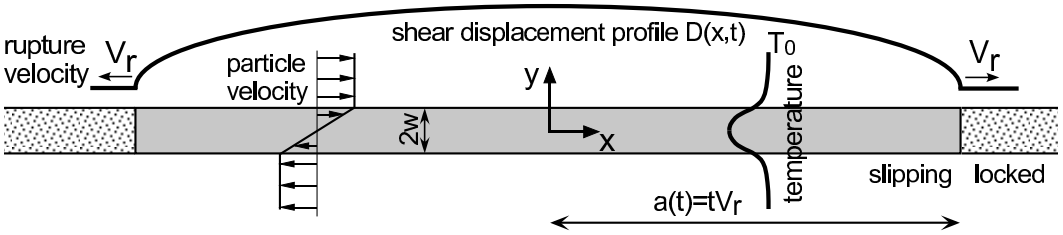

] A schematic view of a dynamically propagating Mode II crack. The crack has a thickness $2w$, and is rupturing bilaterally at a constant velocity $da/dt = V_r$.

Figure 1. [

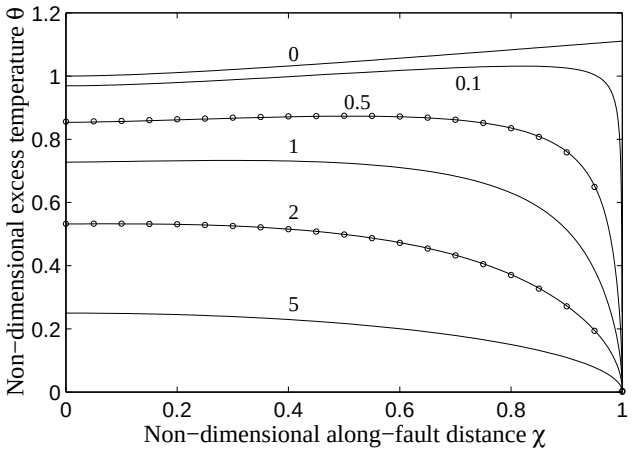

] Variations of the non-dimensional excess temperature $\theta(\chi)$ along a Mode II crack propagating at a constant rupture speed under constant frictional stress. Labels denote the non-dimensional thickness of a slipping zone $\bar{w}$ (see equation (8)). Open circles denote finite difference solutions to equations (3), (2), and (9), for $\bar{w} = 2$ and 0.5.

Figure 2. [

is a characteristic temperature scale for frictional heating assuming a perfectly sharp fault contact (cf. equation (1)).

2.1.1. Linear Elastic Fracture Mechanics approximation

A classic case of a self-similar elastodynamic rupture is a crack slipping under constant dynamic friction, $\sigma_f(x) = \text{const} = \sigma_d$. A zone of inelastic yielding (or, in case of slip on a pre-existing fault, a zone of transition from static to dynamic friction) at the crack tip is neglected. This is the Linear Elastic Fracture Mechanics (LEFM) approximation, in which the displacements along the crack are characterized by a well-known elliptic profile [e.g., *Lawn*, 1993; *Freund*, 1998],

$$D(x,t) = a(t)\epsilon\sqrt{1-\chi^2}, \quad t > 0, |\chi| < 1, \tag{12}$$

and the corresponding slip velocity is

$$\frac{\partial D}{\partial t} = \frac{V_r \epsilon}{\sqrt{1-\chi^2}}. \tag{13}$$

Substituting equation (13) into (5), and making use of the similarity variables (8) and (10), one obtains the following expression for the along-crack temperature distribution in the middle of the slip zone ($y = 0$),

$$\theta(\chi) = \frac{\sqrt{\pi}}{\bar{w}\sqrt{2}} \int_\chi^1 \text{erf}\left[\frac{\bar{w}}{2\sqrt{2(1-\xi)}}\right] \frac{\xi d\xi}{\sqrt{\xi^2-\chi^2}}. \tag{14}$$

Numerical solutions to equation (14) are shown in Figure 2, and further discussed in Appendix A. A family of curves in Figure 2 illustrates a spatio-temporal evolution of temperature on the slipping fault surface. For faults that are thicker than the thermal diffusion lengthscale, or at early stages of rupture (i.e., $\bar{w} > 1$), the temperature increase along the fault is proportional to the amount of slip, as one might expect. For thin faults, or later during the rupture ($\bar{w} \ll 1$), the temperature distribution is very different, with temperature being maximum near the crack tip, and monotonically decreasing from the tip toward the crack center. Note that the instantaneous temperature maximum near the crack tip does not imply cooling of the crack surface behind the tip (see Appendix A). For the non-dimensional fault thickness $\bar{w}$ of the order of unity, the maximum temperature is reached somewhere between the crack center and the rupture front (Figure 2). The semi-analytical solution (14) has been verified with numerical simulations of the boundary value problem (2)-(6) using a finite difference code DifFuse [*Fialko and Rubin*, 1998]. The finite difference calculations are in excellent agreement with the semi-analytic solution (14) (see open circles in Figure 2).

The elevated temperatures near the crack tip produced by thin shear cracks are perhaps surprising, given that shear

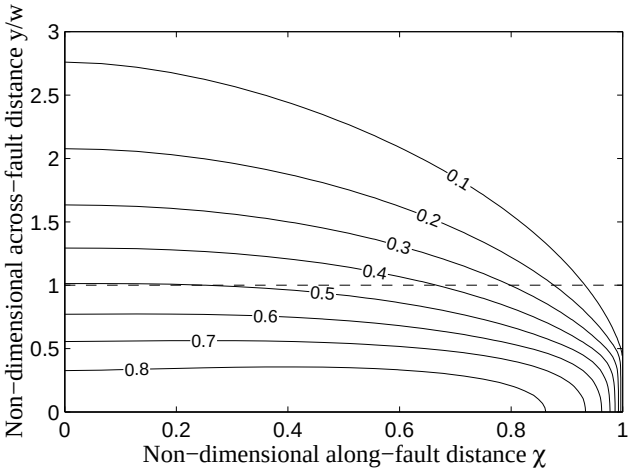

] Temperature field $\theta(\chi, y/w)$ associated with the dynamic propagation of a shear crack given constant friction on the crack surface, for $\bar{w} = 0.5$. The dashed line denotes the boundary of the slip zone.

Figure 3. [

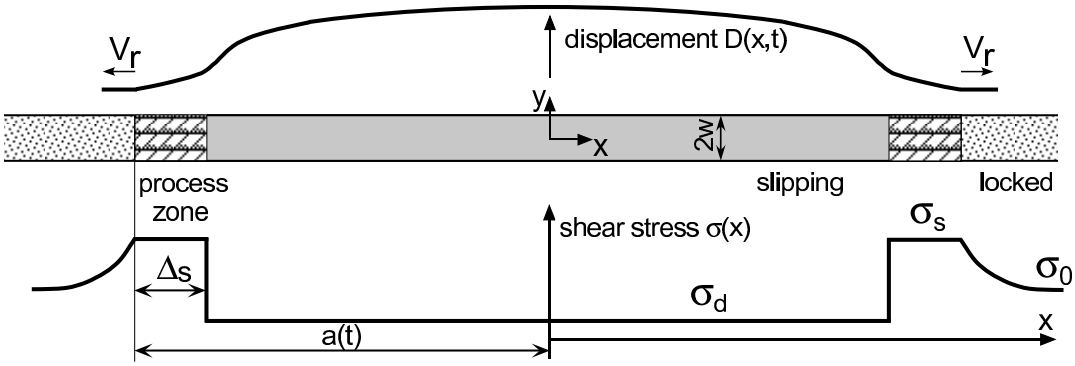

] A two-dimensional plain strain shear crack in an infinite elastic medium. The imposed shear stress at the infinity is σ_0. The crack has a constant thickness $2w$, and a constant interfacial shear stress σ_d. At the crack tips there are process zones having length Δ_T, and shear stress σ_s.

Figure 4. [

displacements are always maximum at the crack center. The inferred anti-correlation between the temperature and the amount of slip stems from a competition between the rates at which the frictional heat is generated at the crack surface, and removed to the ambient rocks by conduction. Generation of frictional heat at the tip of a perfectly sharp LEFM crack is singular as the thickness of the conductive boundary layer is zero, while the slip velocity is infinite (see equation (13)). Nonetheless, the excess temperature at the tip is zero for cracks having finite thickness ($\bar{w} > 0$). For cracks that are much thinner than the conductive boundary layer ($\bar{w} \ll 1$), the temperature field develops a shock-like structure, with the tip temperature exceeding the temperature at the crack center by about 10% (Figure 2). Assuming that the thickness of the slip zone is constant during an earthquake, equation (14) predicts that the maximum temperatures are initially attained at the center of a crack-like shear instability. As the earthquake rupture expands, the temperature maximum may migrate toward the rupture fronts. For the thermal diffusivity of the ambient rocks $\kappa = 10^{-6}$ m^2/s, and rupture durations of $t = 1 - 10$ s (corresponding to the rupture sizes of ∼5-50 km), this transition will occur for faults that have thickness of the order of $\sqrt{2\kappa t} \sim 2 - 5$ mm or less. The critical fault thickness may be larger still if the heat removal from the fault involves some advective transport by the pressurized pore fluids, and the in situ hydraulic diffusivity exceeds the thermal diffusivity κ. Because both the conductive heat transfer and the fluid percolation obey the diffusion equation, the effects of a non-negligible pore fluid flow may be accounted for by using the effective thermal diffusivity $\kappa_e > \kappa$ that lumps the conductive and advective components of heat transfer.

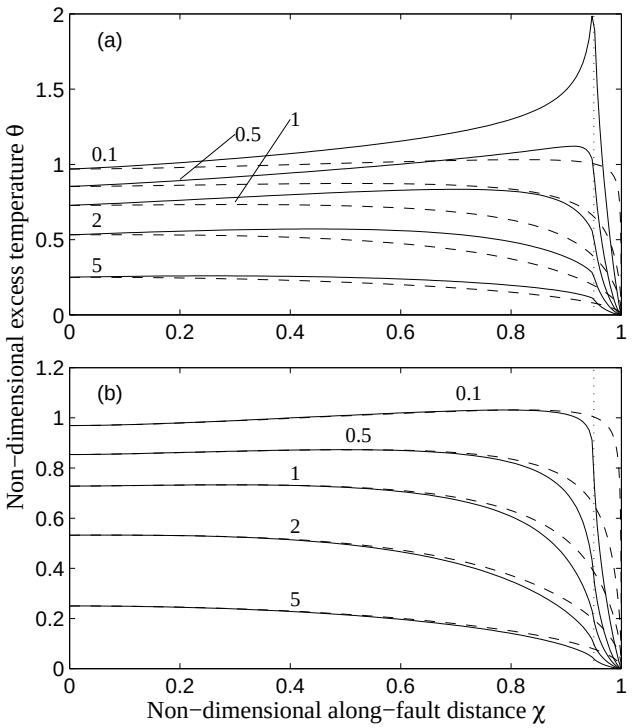

] Temperature distribution along a 2-D shear crack having a cohesive zone at the tip (Figure 4). The ratio of the cohesive zone length to the crack half-length is taken to be 0.05. The base of the cohesive zone is marked by a vertical dotted line. Solid lines denote temperatures in the middle of the gouge layer ($y = 0$), for a range of non-dimensional fault thicknesses $\bar{w}$. Dashed lines denote the respective predictions of the LEFM model (Figure 2). (a) $\sigma_s/\sigma_d = 2.664$. (b) $\sigma_s/\sigma_d = 1$.

Figure 5. [

The distribution of temperature off the crack plane is illustrated in Figure 3 for a particular case $\bar{w} = 0.5$. As expected, the thermal boundary layer develops behind the rupture front, and expands into the surrounding rocks as the crack grows. Heating of thick shear cracks ($\bar{w} \gg 1$) is essentially adiabatic, and gives rise to a nearly isothermal core having thickness of the order of the crack thickness. In the limit of an infinite rupture velocity ($V_r \to \infty$) and uniform slip ($D(x) = \text{const}$), results presented above coincide with the infinitesimally thin fault solutions of *McKenzie and Brune* [1972], and the finite-thickness fault solutions of *Cardwell et al.* [1978] upon replacing ϵV_r with D/t in equation (11), and putting $\chi = 0$ in equation (14).

2.1.2. Effect of the crack tip process zone

Experimental studies of the dynamic crack propagation in various materials including glasses, metals, and polymers reveal the near-tip temperature increases of the order of 10-100 K even for the tensile mode of failure under atmospheric pressure [e.g., *Guduru et al.*, 2001]. These temperature increases are thought to result from plastic working within the process zone at the crack tip [*Rice and Levy*, 1969]. Because the rate of the inelastic energy dissipation at the crack tip is likely to be significantly greater in case of shear failure under high confining pressure, it is instructive to quantify the thermal contribution of the process zone involved in shear rupture. An elegant refinement of the LEFM approach that avoids the stress singularity at the crack tip is the cohesive zone model [*Leonov and Panasyuk*, 1959; *Barenblatt*,

1959; *Dugdale*, 1960]. Originally proposed for tensile (Mode I) cracks, this model postulates that a thin in-plane region of strength degradation exists at the rupture front. Cohesive stresses within the process zone are assumed to balance the driving stresses acting on the developed crack, so that the stresses are finite everywhere. Some macroscopic yield strength σ_s is usually taken to represent the peak stresses attainable within the process zone. The crack growth occurs when a critical displacement D_c is exceeded at the base of the process zone. *Ida* [1972] and *Palmer and Rice* [1973] have adopted the cohesive zone model for shear cracks (in which case it is also referred to as the slip-weakening, or post-yielding model). Although the assumption of a thin in-plane process zone may not be quite valid for either tensile or shear cracks in the Earth [e.g., *Levy et al.*, 1971; *Fialko and Rubin*, 1997; *Manighetti et al.*, 2001], the cohesive zone model provides an instructive end member description of deformation in the near-tip region (e.g., unlike the LEFM model that predicts a blunt crack tip with infinite slip velocity, the cohesive model predicts a cusp-like crack tip with zero slip velocity).

Consider a crack having a cohesive zone with a constant yield stress σ_s. The rest of the crack surface is subject to a constant friction σ_d, as illustrated in Figure 4. Assuming that the crack is rupturing bilaterally at a constant velocity V_r, solutions for the crack displacements and particle velocities (equations (6) and (9)) can be obtained in a closed analytic form (Appendix B). Figure 5a shows solutions to equation (14) for a crack having a cohesive zone that comprises 5% of the crack half-length a, $\Delta_T/a = 0.05$, and a ratio of the stress drop $(\sigma_0 - \sigma_d)$ to dynamic friction σ_d of 0.336. Conditions of equilibrium (equation (B4) in Appendix B) dictate that the corresponding ratio of the yield stress σ_s to dynamic friction σ_d is 2.664. Assuming that all work done against cohesive stresses and static friction in the process zone is ultimately converted into heat, results shown in Figure 5a suggest that the thermal effects of the process zone can be significant. In particular, higher shear stresses within the process zone give rise to temperature increases in the crack tip region that are about a factor of 2 greater compared to predictions of the LEFM model (cf. solid and dashed curves in Figure 5a). Also, the tendency for a shift of the temperature maximum toward the crack tip, as well as the magnitude of the temperature increase are appreciably amplified, especially for thin faults ($\bar{w} < 1$). Simulations in which the size of the process zone is decreased at the expense of a decrease in D_c, and an increase in σ_s, such that the fracture energy is unchanged (see Appendix B), indicate that for the infinitesimally thin cracks the maximum near-tip temperature θ is proportional to the ratio of the process zone friction to the crack friction σ_s/σ_d. It is interesting to note that in the limiting case $\sigma_s/\sigma_d \to \infty$ the process zone becomes infinitesimally small, and the displacements and velocities along the crack asymptotically approach the LEFM solution (eqs. 1 and 13), yet the along-crack temperature distribution significantly deviates from the LEFM solution (Figure 2). This difference is due to the LEFM assumption of no slip (and hence no thermal dissipation) in the region of singular stresses at the crack tip. The magnitude of the near-tip heating is substantially attenuated in case of thick faults (Figure 5a).

The crack tip model assuming a constant cohesive stress predicts that the slip velocity has a weak logarithmic singularity at the base of the process zone $\chi = 1 - \Delta_T/a$ (see equations (9) and (B5)). I point out that the near-tip temperature increases seen in Figure 5a (solid lines) are due to higher stresses, and not the singular particle velocities within the process zone. This conclusion is corroborated by calculations that use the same particle velocities, but assume no increase in friction in the process zone compared to the rest of the crack (i.e., $\sigma_s = \sigma_d$, Figure 5b). In the latter case, the temperature increases predicted by the cohesive zone model are smaller than those predicted by the LEFM model, especially near the crack tip, due to lower rates of the energy dissipation. At distances greater than several process zone lengths behind the rupture front, the temperature increases inferred from the LEFM and the cohesive zone model are similar, as one might expect. Simulations shown in Figure 5b might be relevant if the fracture energy is consumed off the fault plane, or spent on processes other than frictional heating, such as the creation of new surfaces, chemical and phase transformations, etc. Such non-thermal dissipation, however, may be small compared to the amount of work done against friction for earthquakes occuring on mature faults [e.g., *Sibson*, 1980].

2.2. Co-seismic temperature increases due to a self-healing pulse

Detailed near-field observations of a large number of crustal earthquakes indicate that the slip duration, or the so-called rise time, at any point on the fault appears to constitute only a fraction of the total rupture duration [e.g., *Kanamori and Anderson*, 1975; *Heaton*, 1990; *Beroza and Mikumo*, 1996; *Olsen et al.*, 1997]. This is inconsistent with the crack-like models of the earthquake rupture (e.g., Figure 1) which predict that the slip should continue until the rupture front has ceased propagating (equation (9)). In this section I consider frictional heating associated with the pulse-like seismic ruptures. The geometry of the problem

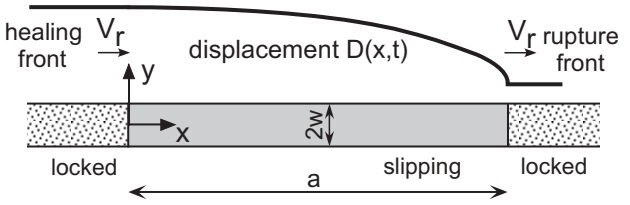

] A self-healing pulse having length a propagating at a constant speed V_r. The remote shear stress is σ_0, and frictional stress on the slipping surface is σ_d. The pulse length is a, and the thickness of the slipping zone is $2w$.

Figure 6. [

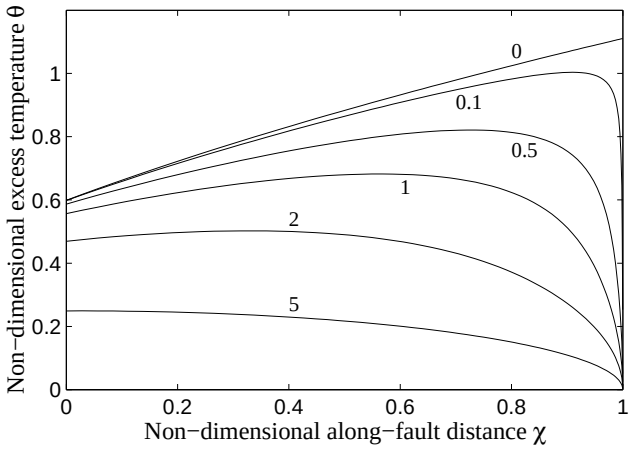

] Variations of the non-dimensional excess temperature $\theta(\chi)$ along a self-healing pulse. Labels denote the non-dimensional thickness of a slipping zone $\bar{w}$ (see equations (18)).

Figure 7. [

is shown in Figure 6. As in the previous analysis, it is assumed that the slipping zone has a constant thickness $2w$, and a constant dynamic friction σ_d. The rupture front propagates at velocity V_r, and is trailed by the healing front at a distance a. Elastodynamic solutions to this problem were discussed by *Yoffe* [1951] for a Mode I pulse, and *Freund* [1979] for a Mode II pulse. For a self-healing pulse having a constant length a, I anticipate steady state solutions for the co-seismic temperature field in the reference frame of the moving rupture front. The appropriate similarity variables are

$$\text{along-fault coordinate} \quad \chi = \frac{x - tV_r}{a} + 1, \tag{15}$$

$$\text{non-dimensional fault thickness} \quad \bar{w} = \sqrt{\frac{2V_r}{a\kappa}}w, \tag{16}$$

$$\text{non-dimensional temperature} \quad \theta = \frac{T - T_0}{\hat{T}}, \tag{17}$$

$$\hat{T} = \frac{\sigma_d \epsilon}{c\rho}\sqrt{\frac{aV_r}{\pi\kappa}}. \tag{18}$$

The along-fault displacements and the rate of slip are assumed to obey the following relationships,

$$D(\chi) = a\epsilon\sqrt{1-\chi^2}, \tag{19}$$

$$\frac{\partial D}{\partial \chi} = \frac{V_r \epsilon \chi}{\sqrt{1-\chi^2}}. \tag{20}$$

That is, the LEFM-like asymptotic behavior is assumed at the fault tip ($\chi = 1$). Because the assumption of a constant dynamic friction does not warrant fault healing [*Freund*, 1979; *Heaton*, 1990], the latter is artificially imposed at the trailing edge ($\chi = 0$); possible physical mechanisms of fault healing are discussed in Section 3. Upon non-dimensionalization using variables (18), equation (5) gives rise to the following formula for the along-fault temperature variations in the middle of the slip zone ($y = 0$) given the slip velocities (20),

$$\theta(\chi) = \frac{\sqrt{\pi}}{\bar{w}\sqrt{2}}\int_{\chi}^{1} \mathrm{erf}\left[\frac{\bar{w}}{2\sqrt{2(\chi-\xi)}}\right]\frac{\xi d\xi}{\sqrt{1-\xi^2}}. \tag{21}$$

Solutions to equation (21) are shown in Figure 7 (also, see Appendix A). The near-tip structure of the temperature field due to a steady state pulse is similar to that due to a self-similar expanding crack (cf. Figures 2 and 7). At the leading edge of an infinitesimally thin shear pulse there is a thermal shock of amplitude $\hat{T}$ (equation 18). The fault temperature monotonically decreases toward the healing front, where the temperature falls to about one half of the maximum value (Figure 7 and Appendix A). For "thick" pulses ($\bar{w} \gg 1$), the fault temperature increases toward the healing front proportionally to the amount of slip. For intermediate fault thicknesses of the order of unity, the initial fault heating behind the rupture front eventually gives way to cooling before the arrival of the healing front. This behavior is qualitatively different from the temperature variations on a surface of an expanding crack, which indicate a progressive heating at every point along the crack as long as the rupture continues (Appendix A). The inferred cooling toward the healing front of the steady state pulse for $\bar{w} < 5$ is caused by a decreasing heat generation due to a vanishing slip velocity, and efficient removal of heat by thermal diffusion. For the characteristic rise times a/V_r of the order of seconds, the steady state LEFM pulses need to be thicker than $5\sqrt{2\kappa a/V_r} \approx 1$ cm to experience maximum temperatures at the healing front. Simulations including a process zone at the leading edge of a pulse predict a near-tip temperature field that is analogous to that due to a self-similar crack (e.g., Figure 5a).

3. Discussion

Theoretical modeling of the co-seismic frictional heating (Figures 2 and 7) indicates that the effective thickness of the earthquake slip zone controls not only the magnitude of the temperature increase, but also where on a fault the maximum temperature is reached. The intrinsic lengthscale that separates the thin fault heating (characterized by the inverse proportionality between the fault temperature and the amount of slip) from the thick fault heating (in which the temperature is directly proportional to slip) is the thickness of the thermal boundary layer $\sqrt{2\kappa t}$. For typical rise times of moderate-to-large earthquakes of $t = 1 - 10$ s, the corresponding lengthscale is of the order of several millimeters (assuming a purely conductive cooling) or greater (if the heat advection by pore fluids is non-negligible). There is field evidence that the primary slip surfaces of major crustal faults may have widths of the order of 1 cm or less [e.g., *Sibson*, 1975; *Suppe*, 1985; *Chester and Chester*, 1998]. While faults are also known to be associated with considerably wider ($1 - 10^3$ m), and possibly scale-dependent zones of damaged rock with reduced effective elastic moduli [*Scholz*, 1990; *Ben-Zion*, 1998; *Fialko et al.*, 2002; *Vidale and Li*, 2003], it is conceivable that these macroscopic compliant fault zones do not accommodate significant inelastic shear strain. In particular, wide damage zones may be a result of volumetric deformation generated off the fault plane by passing rupture fronts, and/or multiple earthquakes on subparallel slip planes within the fault zone. The characteristic thickness of a layer that accommodates the bulk of slip in individual earthquakes is poorly known, especially at the seismogenic depths. Laboratory experiments and theoretical modeling indicate that shear deformation of rocks tends to produce an extreme slip localization that is ultimately limited by the rock microstructure (e.g., grain size) [*Sammis et al.*, 1987; *Mora and Place*, 1994; *Scruggs and Tullis*, 1998; *Sleep et al.*, 2000]. If so, both the thin and thick fault

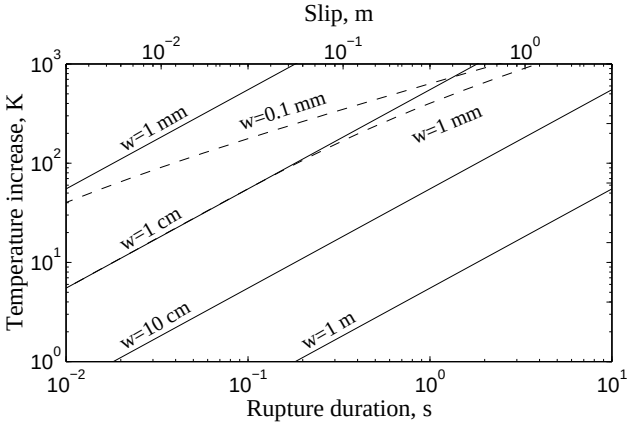

] Co-seismic temperature increases on the surface of a Mode II LEFM crack, as a function of the rupture duration t, and the slip zone thickness $2w$. Solid lines correspond to the dynamic friction $\sigma_d = 10^8$ Pa, and dashed lines correspond to $\sigma_d = 10^7$ Pa. All calculations assume $V_r = 3$ km/s, $\epsilon = 10^{-4}$, $\kappa = 10^{-6}$ m^2/s, and $c = 10^3$ J/kg/K.

Figure 8. [

heating regimes discussed above might be relevant to earthquakes.

The magnitude of maximum temperature perturbations due to frictional heat dissipation on a surface of a crack-like earthquake rupture is shown in Figure 8 for a range of the slip zone thicknesses $2w$. A transition from a thick to a thin fault heating regime results in a change in scaling of the maximum temperature with time from $\Delta T \propto t$ to $\Delta T \propto \sqrt{t}$, respectively. This transition occurs at a characteristic time $t_c = 2w^2/\kappa$ (i.e., corresponding to $\bar{w} = 1$). Using the laboratory-derived estimates of fault friction at the seismogenic depths of the order of the $\sigma_d = 10^8$ Pa [e.g., *Byerlee*, 1978], solutions to equation (14) suggest that faults that are thinner than a few meters are capable of generating the co-seismic temperature increases of the order of 10-10^3K. In case of high friction, the melting temperatures are likely to be reached before the transition from a thick to a thin fault heating regime, even for faults that are as thin as a few millimeters (solid lines in Figure 8). Only extremely localized faults slipping under a low dynamic friction are predicted to experience such a transition (see dashed lines in Figure 8 corresponding to $\sigma_d = 10^7$ Pa). Note that the magnitude of the temperature increase is proportional to the dimensionless group $\sigma_d V_r \epsilon w / c\rho\kappa$ (equations 10 and 11), so that the maximum temperatures due to loading conditions other than those assumed can be readily obtained by a simple rescaling of the dimensional results shown in Figure 8 (e.g., a factor of two decrease in the assumed strain drop ϵ would result in a factor of two decrease in ΔT, and so on).

As one can see from Figure 8, thermal effects are expected to be especially significant for faults with highly localized slip zones (i.e., having characteristic thicknesses of the order of 0.1 m or less) [also, see *Sibson*, 1977; *Cardwell et al.*, 1978; *Kanamori and Heaton*, 2000]. Theoretical results presented in Section 2 describe thermal evolution of the slipping fault prior to the onset of the thermally-induced variations in friction, and become inapplicable after the the constitutive properties of the slipping fault surface are substantially modified by the co-seismic temperature perturbations. Thermally-activated mechanisms that may affect the fault resistance to shear include thermal pressurization [*Sibson*, 1973; *Lachenbruch*, 1980; *Mase and Smith*, 1987; *Segall and Rice*, 1995], frictional melting [*Jeffreys*, 1942; *McKenzie and Brune*, 1972; *Sibson*, 1975; *Maddock*, 1986], and flash heating of fault asperities [*Rice*, 1999]. These mechanisms are generally believed to result in a substantial fault weakening, and increases in the earthquake stress drop. Given a possibility of a feedback between the dynamic fault friction and the co-seismic heating, calculations shown in Figures 2, 5, and 7 predict quite different slip histories for thick and thin faults. For thick ($\bar{w} > 1$) crack-like ruptures (Figure 1), the initial phase of unstable slip is expected to have a relatively low stress drop. The onset of the thermally-induced weakening occurs around the earthquake nucleation site, and is followed by a secondary rupture phase with a higher stress drop propagating toward the rupture front. The initiation of the secondary high stress drop phase corresponds to a characteristic rupture size $2w\Delta T c\rho/\sigma_d\epsilon$, where σ_d is the dynamic fault friction prior to thermal weakening, and ΔT is the activation temperature. Assuming the fault thickness of 10 cm, the activation temperature of the order of 10^2 K, and the fault friction of the order of 10^8 Pa [*Byerlee*, 1978], the corresponding rupture size is of the order of hundreds of meters to kilometers for typical earthquake strains of $10^{-4} - 10^{-5}$, respectively. There is no tendency for a transition from a crack-like to a pulse-like rupture mode, as the central part of a crack continues to weaken with increasing temperature. Pulse-like ruptures that are thicker than $5\bar{w}$ (~ 1 cm assuming conductive cooling and typical rise times of the order of seconds) are likely to experience highest temperatures at the healing front, so that in case of thermal weakening and thick faults, healing is ought to be caused by non-thermal mechanisms. In contrast, thin ($\bar{w} < 1$) elastodynamic instabilities may thermally weaken near the rupture front, so that the region of high stress drop will propagate in the direction opposite to the rupture direction until it reaches the nucleation site. The initiation of the secondary high stress drop phase corresponds to a characteristic rupture size $\pi\kappa(\Delta T c\rho)^2/V_r(\sigma_d\epsilon)^2$. Note that the thermal weakening can occur nearly instantaneously along a significant portion of a slipping fault (Figures 2 and 7). In case of an extreme slip localization, or provided that the tip process zone substantially perturbs the near-tip temperature field, the temperature weakening might be one of the physical mechanisms causing healing of the pulse-like earthquake ruptures. However, there is still no tendency for a transition from a crack to a pulse mode of propagation.

If the initial frictional heating does not result in a substantial fault weakening (e.g., in the absence of pore fluids, or due to high dynamic permeability of the fault gouge zone during rupture), continued slip on faults that are thinner than 1-10 cm may produce temperature increases of the order of several hundred degrees (Figure 8), sufficient to cause melting. While it is commonly believed that the onset of melting results in a dramatic drop in the fault friction [*Jeffreys*, 1942; *McKenzie and Brune*, 1972], there exist theoretical arguments and laboratory data suggesting that a transition from frictional to viscous sliding may be in fact accompanied by considerable increases in the dynamic fault strength.

For shallow crustal faults, the frictional stress on a fault σ_f is presumed to obey an empirical Mohr-Coulomb relationship,

$$\sigma_f \propto \mu(\sigma_n - p), \tag{22}$$

where μ is the effective coefficient of friction, σ_n is the fault-normal stress, and p is the pore fluid pressure. The direct proportionality between the shear and normal stresses in equation 22 is a consequence of an imperfect contact between the sliding rock interfaces [*Bowden and Tabor*, 1954; *Byerlee*, 1978]. Laboratory experiments suggest that most of the resistance to slip comes from a relatively small contact area between riding asperities that are likely to sustain much higher stress than σ_f [e.g., *Teufel and Logan*, 1978]. Given sufficiently high slip rates, temperature increases on such contacts may result in weakening of the asperities (e.g., via plasticity, dislocation creep, microscopic melting, etc.). This weakening may manifest itself in an apparent reduction in the frictional stress σ_f [*Rice*, 1999]. However, as the asperity contacts are progressively weakened and flattened, the total contact area between the mating surfaces is expected to increase, both at the expense of the thermo-mechanical erosion of the asperities, and due to accumulation of melt in the "lowlands". This increase in the total contact area may in principle offset the reduction in the peak stress supported by the asperities, so that the overall frictional resistance to sliding may increase. A spectacular increase in shear stress at the onset of macroscopic melting has been observed in the rotary shear experiments of *Tsutsumi and Shimamoto* [1997] at sliding velocities of 70 cm/s. A similar transient strengthening is also reported in the high-speed rock sliding experiments of *Spray* [1993].

After a continuous film of melt is formed on a fault surface, most of the resistance to slip comes from viscous deformation of a melt layer, rather than a Mohr-Coulomb friction (22). Assuming that the melt has a Newtonian rheology, the viscous stress σ_v due to simple shear of fluid between two parallel surfaces (Couette flow) is given by [e.g., *Turcotte and Schubert*, 2002, p.229]

$$\sigma_v = \frac{\dot{D}\eta}{2w}, \tag{23}$$

where $\dot{D}$ is the sliding velocity (hereafter, the dot operator denotes differentiation with respect to time t, $\dot{f} = \partial f/\partial t$), η is the dynamic melt viscosity, and $2w$ is the thickness of the melt layer. Viscosity of silicate melts varies greatly. For super-solidus crystal-free granitic melts, η is of the order of $10^4 - 10^8$ Pa s, depending on a volatile content [*McBirney*, 1993; *Rubin*, 1995]. A comparison of equations 22 and 23 suggests that frictional fusion does not necessarily imply a drop in shear stress on a fault surface. For example, assuming $\dot{D} = 1$m/s, $\eta = 10^6$ Pa s, and $2w = 1$ mm, from equation (23) one obtains a shear stress of $\sim$1 GPa, of the order of the theoretical strength of crystalline rocks, and an order of magnitude greater than the average Mohr-Coulomb failure stress for the upper crust [equation (22); *Scholz*, 1990, p. 136]. Mafic melts have considerably lower viscosities $O(10 - 10^3)$ Pa s, and are likely to provide smaller viscous resistance during incipient melting. Nonetheless, increases in the apparent frictional resistance of gabbro reported in the high shear rate experiments of *Tsutsumi and Shimamoto* [1997] suggest that melting of mafic rocks may as well result in viscous braking. Factors that might contribute to increases in the effective viscosity of frictional melts include a high volume fraction of solid particles, viscoelastic effects, and non-linear melt rheology at high strain rates.

If the onset of melting is accompanied by increases in shear stress exceeding the static friction, or the intrinsic rock strength, the fused fault may be abandoned, and the slip may be transferred to a new sub-parallel plane. Side-wall rip-out structures associated with some pseudotachylite-bearing faults [e.g., *Swanson*, 1992] may be an example of such a thermally-induced "defocusing" of seismic slip. Similarly, *Otsuki et al.* [2003] describe sub-parallel sequences of millimeter-wide pseudotachylite layers in the exposed core of the Nojima fault in southwest Japan. While they suggest that the total number of the observed pseudotachylite layers is representative of the number of past earthquakes on the fault, it is possible that the multiple melt layers could be produced during individual earthquakes by slip transfer due to viscous braking. The progressive jumping of the slip surfaces in the fault-perpendicular direction might contribute to an increase in the effective fracture energy of an earthquake. If the available driving stress is insufficient to initiate sliding on a new surface, the slip velocity will initially decrease. The subsequent evolution of slip depends on the thickness of the formed melt layer. Provided that the driving shear stress is constant, there is a critical thickness that separates the layers that monotonically decelerate and ultimately freeze from those that eventually accelerate and localize strain, resulting in a so-called thermal runaway [*Fialko*, 1999]. The timescale corresponding to the transition from viscous braking to lubrication is controlled by rheologic properties of the friction-generated melts. A necessary condition for melt lubrication to occur is that the timescale for thermal runaway is small compared to the duration of seismic slip. A detailed analysis of the thermodynamics of frictional melting is hindered by the lack of empirical data pertinent to the rheologic properties of silicate melts at strain rates $O(10^2 - 10^4)$ s^{-1} that might be typical of seismic slip.

The transient thermal strengthening may affect the earthquake rupture in several ways. If the near-solidus temperatures are first reached near the rupture front (i.e., for $\bar{w} < 1$), they might give rise to fault branching and increases in the effective fracture energy, as discussed above. If the onset of viscous braking occurs near the crack center (i.e, for $\bar{w} > 1$), the resulting patch of high friction is expected to extend toward the rupture front. If the patch size becomes large compared to the crack size, the crack propagation may be ultimately terminated. Faults having thickness of the order of the thermal boundary layer, $\bar{w} \sim O(1)$, are most vulnerable for the thermal lock-up (see Figure 2). Finally, if the length of the crack segment between the rupture front and the melting front is greater than the critical length for the dynamic instability (i.e., the length of an equilibrium crack on the verge of propagation), there may be a transition from the bi-lateral crack to the uni-lateral pulse propagation. That is, as the central section of the crack becomes permanently locked once the temperature approaches solidus, the expanding melting front becomes the healing front of a pulse of slip trailing the rupture front. In this scenario, the slip occurs as long as the fault surface remains sub-solidus. A necessary condition for the pulse healing due to thermal strengthening is that the fault has to be sufficiently thick compared to the diffusion lengthscale (to ensure the along-fault increases in temperature, see Figures 2 and 7), yet sufficiently thin to raise temperature to solidus (see equations 1 and 18),

$$5\sqrt{2\kappa t} < 2w < \frac{\sigma_d D}{\Delta T c \rho}. \tag{24}$$

Equation 24 suggests the following lower bound on the level of the dynamic friction σ_d,

$$\sigma_d > \frac{5\sqrt{2\kappa t}\Delta T c \rho}{D}. \tag{25}$$

All parameters on the right hand side of equation 25 can be either inferred from laboratory measurements (i.e., the thermophysical constants κ, c, and ρ), or determined from seismic data (i.e., the rise time t and the slip amplitude D). Table 1 lists the observational data for several pulse-like earthquake ruptures compiled by *Heaton* [1990], along with the respective estimates of the minimum dynamic fault friction calculated using equation (25), assuming the activation temperature $\Delta T = 500$ K. While the seismic energies of earthquakes listed in Table 1 differ by more than two orders of magnitude, the inferred lower bound on the dynamic friction is essentially independent of the earthquake size, and is found to be of the order of several megapascals. This is comparable to the earthquake stress drops, but significantly smaller than the average Mohr-Coulomb strength of the upper crust (assuming Byerlee's friction and hydrostatic pore pressures). Assuming that viscous braking is the mechanism responsible for pulse healing, it can be argued that the actual dynamic friction cannot significantly exceed the lower bound (25). This is because an increase in the fault thickness necessary to offset the higher friction imply an increase in the thickness of the fused layer, which may ultimately render the viscous braking inefficient (equation 23). Other mechanisms proposed to explain the short duration of seismic slip, and the pulse-like mode of rupture include stress heterogeneities [e.g., *Day*, 1982; *Beroza and Mikumo*, 1996], strong velocity weakening [*Perrin et al.*, 1995; *Zheng and Rice*, 1998], and slip between dissimilar material interfaces [*Ben-Zion and Andrews*, 1998]. It is possible that a variety of mechanisms may be responsible for the observed short rise times of large earthquakes.

Field observations of pseudotachylites (veins of dark aphanitic rock in the cores of the exposed fault zones) are evidence that at least in some cases the co-seismic frictional heating is sufficiently robust to produce macroscopic melting [*Price*, 1970; *Sibson*, 1975; *Wallace*, 1976; *Swanson*, 1992; *Wenk et al.*, 2000]. However, pseudotachylites are not commonly found in the majority of the exposed fault zones. Assuming hydrostatic pore pressures and Byerlee's friction [*Byerlee*, 1978], melting during moderate-to-large earthquakes can be prevented only if seismic slip is distributed over a zone having thickness of the order of tens of centimeters to meters (or greater). Even if the fault friction is low (e.g., σ_d <20 MPa, sufficient to satisfy the heat flow paradox of the San Andreas fault [*Brune et al.*, 1969; *Lachenbruch and Sass*, 1980]), melting seems unavoidable if the thickness of

a slipping region is less than a few centimeters (Figure 8). The apparent paucity of pseudotachylites in thin cores of the exposed faults that presumably produced earthquakes in the past [e.g., *Chester and Chester*, 1998] therefore constitutes what may be called a second, or a local heat flow paradox. One possible explanation is that pseudotachylites might ubiquitously form in situ, but not be readily preserved in the exhumed rocks [*Wallace*, 1976]. The absence of melting might be also interpreted as evidence for extremely low shear stresses associated with faulting [e.g., *Price*, 1970]. An alternative possibility is that the viscous braking arrests slip during early stages of melting. This implies that the fault fusion is generally a self-terminating process, and the formation of macroscopic melt veins may require special circumstances (e.g., high shear stress, favorable thickness of the slip zone, and volatile-rich frictional melt). If so, greater efforts may be warranted for obtaining field constraints on the maximum temperatures experienced by seismogenic faults.

4. Conclusions

I presented semi-analytic solutions for fault heating during seismic instabilities. The thermal history of seismic slip is deduced for 2-D models of the elastodynamic shear rupture. Self-similar solutions for the temperature evolution on the fault surface are obtained for the case of a Mode II crack, and a self-healing pulse having a constant thickness of the slip zone, and rupturing at a constant velocity. Provided that friction on a slipping fault is constant (or variations in friction are small compared to the subsequent thermally-induced stress perturbations), the along-fault temperature distribution depends on a ratio of the fault thickness to the thickness of the thermal boundary layer. Faults that are thicker than the thermal boundary layer experience maximum temperatures in the center (in case of a bi-laterally rupturing crack), or at the healing front (in case of a pulse-like rupture). Conversely, faults that are thinner than the thermal boundary layer generate maximum temperatures at the rupture front. For the observed earthquake rise times of the order of seconds, and using the laboratory values of the thermal diffusivity of $\sim 10^{-6}$ m^2/s, the corresponding transitional thickness is of the order of millimeters. The near-tip temperature increases may be also encouraged by high shear stresses acting in the crack tip process zone. The thermal effect of the process zone is inversely proportional to the fault thickness.

The inferred along-fault temperature variations may affect the pattern and amount of seismic radiation, depending on whether the fault rheology is temperature weakening or temperature strengthening. The experimental measurements of the rate and state dependent friction properties indicate a modest temperature strengthening at low slip rates [e.g., *Blanpied et al.*, 1998]. However, it is believed that such strengthening is offset by velocity weakening at high (seismic) slip rates. Other models that explicitly consider the effect of temperature on the dynamic fault friction, including the thermal pressurization, and frictional melting, assume that faults generally weaken at elevated temperatures. However, few available measurements of dynamic friction at the seismic slip velocities reveal that the onset of macroscopic melting (i.e., a transition from a dry friction to a viscous rheology) may result in significant increases in the fault resistance to shear. This resistance likely stems from increases in the effective contact area between the fault surfaces, and high viscosities of the frictionally generated silicate melts. Transient increases in viscous stresses at the onset of frictional fusion (termed "viscous braking") may affect the earthquake ruptures in several ways, including (1) de-focusing of seismic slip, (2) transition from a crack-like to a pulse-like rupture mode, or (3) ultimate rupture arrest. This implies that frictional fusion may be a self-terminating process, which may explain a relative paucity of pseudotachylites in the exposed fault zones. Assuming that the viscous braking is a dominant mechanism for healing of narrow slip pulses, a combination of theoretical results presented in this paper with seismologically-determined characteristics of several pulse-like earthquakes [*Heaton*, 1990] allows one to place a lower bound on the dynamic fault friction of the order of several megapascals.

The semi-analytic solutions for the thermal evolution of shear instabilities have been verified with the fully numerical finite difference simulations. The finite difference model can be readily used to perform more sophisticated simulations accounting for, e.g., the along-fault variations in the dynamic friction and the thickness of the gouge layer, as well as the coupling between the local shear stress, temperature, and slip rate. Such simulations are not yet warranted due to a lack of empirical data describing the fault zone properties and the characteristic seismic strain rates. Further understanding of the energetics of faulting requires laboratory investigations of the rheologic properties of the frictionally generated melts at high strain rates, and constraints from field observations on (i) the range of fault thicknesses involved in individual slip events, and (ii) the average temperatures attained on the surface of exposed faults that presumably generated seismic events in the past.

The feedbacks between the frictional heat generation, the temperature dependent fault resistance to shear, and the seismic radiation are likely to result in a wide range of possible behaviors, implying a significant richness and complexity in the earthquake rupture dynamics. As seismic and geodetic observations in the near field of large earthquakes provide an increasingly detailed view of the rupture histories [*Wald and Heaton*, 1994; *Beroza and Mikumo*, 1996; *Olsen et al.*, 1997; *Ide and Takeo*, 1997], future models of the earthquake source may benefit from explicitly considering the thermodynamic effects of faulting.

Acknowledgments. I thank Freeman Gilbert and Yakov Khazan for comments on the early version of this manuscript, and Glenn Ierley for help with evaluating integral (A4) in Appendix A. The manuscript (and the author) greatly benefited from thoughful reviews by Steve Day, Rajesh Chanpura, and Associate Editor Leonid Germanovich. This work was supported by NSF (grant EAR-0338061) and Vetlesen Foundation. Numerical codes used in this study are available from the author.

Appendix A: Solutions for co-seismic heating in the limit of zero fault thickness

For an infinitesimally thin LEFM crack ($\bar{w} \to 0$) one may take advantage of the limiting relationship

$$\lim_{x\to 0} \frac{\mathrm{erf}(xk)}{x} = \frac{2}{\sqrt{\pi}} k, \tag{A1}$$

and reduce equation 14 to

$$\theta(\chi) = \frac{1}{2} \int_{\chi}^{1} \frac{d\xi}{\sqrt{1-\xi}\sqrt{1-\left(\frac{\chi}{\xi}\right)^2}}. \tag{A2}$$

A further evaluation of equation A2 leads to elliptic integrals, and so one must resort to numerical integration. The latter is somewhat complicated by the fact that the integrand is singular on both limits of integration. Therefore special treatments, such as analytical removal of singularities, and custom integration quadratures, are needed for an accurate solution to equation (A2).

A numerical solution to equation (A2) is shown in Figure 2 (case $\bar{w} = 0$). The temperature on a perfectly sharp

Mode II crack monotonically increases from the crack center ($\chi = 0$) toward the crack tip ($\chi = 1$). The exact values of the non-dimensional temperature at the crack center and the crack tip can be readily obtained from equation (A2),

$$\theta(0) = \frac{1}{2}\int_0^1 \frac{d\xi}{\sqrt{1-\xi}} = 1, \tag{A3}$$

$$\theta(1) = \frac{1}{2\sqrt{2}} \lim_{\chi\to 1} \int_\chi^1 \frac{d\xi}{\sqrt{1-\xi}\sqrt{\xi-\chi}} = \frac{\pi}{2\sqrt{2}} \approx 1.1107. \tag{A4}$$

The temperature at the crack tip exceeds the temperature at the crack center by about 10%, in agreement with numerical calculations shown in Figure 2.

Note that the along-crack increases in the dimensionless temperature θ inferred for thin shear cracks (Figure 2) do not imply that the crack walls cool off behind the propagating rupture front. It can be shown using equations (8) and (14) that the time derivative of the (dimensional) temperature,

$$\frac{\partial T}{\partial t} = \frac{\partial(\theta\hat{T})}{\partial t} = \frac{\partial \hat{T}}{\partial t}\theta + \frac{\partial \chi}{\partial t}\frac{\partial \theta}{\partial \chi}\hat{T} = \frac{\hat{T}}{t}\left(\frac{\theta}{2} - \chi\frac{\partial\theta}{\partial\chi}\right), \tag{A5}$$

is positive at any point along the crack. In particular, for perfectly sharp cracks ($\bar{w} = 0$), $\theta/2 > 0.5$, while $\chi\partial\theta/\partial\chi < \max(\partial\theta/\partial\chi) < 0.2$ (see Figure 2), so that the temperature on the crack surface $T(x, 0, t)$ steadily increases with time. The characteristic rate of the temperature increase is proportional to the inverse square root of time, $\partial T/\partial t \propto t^{-1/2}$, as expected of a conduction-dominated heat transfer [e.g., *Carslaw and Jaeger*, 1959].

Let's now consider a temperature rise due to an infinitesimally thin self-healing pulse. For the case $\bar{w} \to 0$, equation 14 becomes

$$\theta(\chi) = \frac{1}{2}\int_\chi^1 \frac{\xi d\xi}{\sqrt{\xi-\chi}\sqrt{1-\xi^2}}. \tag{A6}$$

A numerical solution to equation A2 is shown in Figure 7 ($\bar{w} = 0$). The non-dimensional temperature at the healing front of the pulse is obtained by putting $\chi = 0$ in equation (A6),

$$\theta(0) = \frac{1}{2}\int_0^1 \frac{\sqrt{\xi}d\xi}{\sqrt{1-\xi}} = \frac{\sqrt{\pi}\Gamma(3/4)}{\Gamma(1/4)} \approx 0.5991, \tag{A7}$$

where Γ is the factorial function, $\Gamma(x) = \int_0^\infty t^{x-1}e^{-t}dt$. For $\chi = 1$ (i.e., at the pulse tip), equation (A6) reduces to (A4). Thus, for an infinitesimally thin self-healing pulse, the temperature at the rupture front exceeds that at the healing front by almost a factor of two (Figure 7).

Unlike in the case of a self-similar crack, the instantaneous temperature behind the rupture front of a self-healing pulse may either increase or decrease, depending on the non-dimensional pulse thickness $\bar{w}$,

$$\frac{\partial T}{\partial t} = \frac{\partial \chi}{\partial t}\frac{\partial \theta}{\partial \chi}\hat{T} = -\frac{V_r}{a}\frac{\partial\theta}{\partial\chi}\hat{T}. \tag{A8}$$

Equations (A8) and (18) indicate that the temperature evolution on the surface of a steady state pulse is controlled by the slope of the $\theta(\chi)$ curve, implying heating for $\partial\theta/\partial\chi < 0$ ($\bar{w} \gg 1$), and cooling for $\partial\theta/\partial\chi > 0$ ($\bar{w} < 1$, see Figure 7).

Appendix B: Analytic expressions for particle velocities due to a 2-D crack with a slip-weakening process zone

Because the equilibrium equations are identical for Mode I (tensile) and Mode II (in-plane shear) loading, solutions for Mode II cracks can be readily obtained from the Mode I solutions by replacing normal stresses and displacements with shear stresses and displacements.

Let $\sigma(x)$ be a distribution of shear stresses acting on a crack surface, and σ_0 be a far-field shear stress prior to faulting. The crack slip that satisfies equations of elastic equilibrium is given by [e.g., *Khazan and Fialko*, 1995, equation (11)],

$$D(x) = \frac{2a(1-\nu)}{\pi\mu}\int_x^a \sqrt{a^2-\tau^2}d\tau \int_{-a}^a \frac{\sigma(\xi)d\xi}{(\tau-\xi)\sqrt{a^2-\xi^2}}. \tag{B1}$$

The finiteness of stresses at the crack tip is ensured by requiring that the stress intensity factors at the crack tips are zero,

$$\int_{-a}^a \frac{\sigma(x)-\sigma_0}{\sqrt{a^2-x^2}}dx = 0. \tag{B2}$$

(see *Khazan and Fialko* [1995] for details). In general, solutions to equation (B1) may be obtained numerically for an arbitrary slip-weakening law and a driving stress distribution ($\sigma_0 - \sigma(x)$) that satisfies constraint (B2).

For a piece-wise constant symmetric distribution of frictional stresses on the crack surface, as shown in Figure 4 in the main text,

$$\sigma(x) = \begin{cases} \sigma_d, & |x| < a - \Delta_T \\ \sigma_s, & a - \Delta_T \le |x| \le a, \end{cases} \tag{B3}$$

evaluation of (B2) provides an expression for the length of the equilibrium process zone Δ_T,

$$\frac{\Delta_T}{a} = 1 - \sin\left[\frac{\pi}{2}\frac{\sigma_s-\sigma_0}{\sigma_s-\sigma_d}\right]. \tag{B4}$$

Equation (B1) can be as well integrated analytically yielding expressions for both the displacement and the displacement gradient as functions of the non-dimensional along-crack coordinate $\chi = x/a$,

$$\frac{\partial D(\chi)}{\partial\chi} = -\frac{2a(1-\nu)}{\pi\mu}(\sigma_s-\sigma_d)\left[F(\chi, L) - F(\chi, -L)\right], \tag{B5}$$

$$D(\chi) = \frac{2a(1-\nu)}{\pi\mu}(\sigma_s-\sigma_d)\left[(\chi+L)F(\chi, L) - (\chi-L)F(\chi,-L)\right], \tag{B6}$$

where $L = 1 - \Delta_T/a$ is the non-dimensional length of the crack behind the process zone, and function F is given by

$$F(U, V) = \log\left|\frac{\sqrt{(1-U^2)(1-V^2)} + UV + 1}{U+V}\right|. \tag{B7}$$

Particle velocities on the crack surface can then be calculated using equation (9) in the main text.

Although equilibrium solutions presented above describe quasi-static cracks, they can be also used to analyze the dynamic crack propagation provided certain conditions, such as the constant subsonic rupture velocity, and small-scale yielding (i.e., $1-L \ll 1$) are met [*Broberg*, 1978; *Rice*, 1980].

In a coordinate frame of a moving crack tip, the near-tip displacement profile experiences a relativistic shrinking by a factor β that is a function of the ratio of the rupture velocity V_r to a limiting velocity V_l (V_l being the Rayleigh wave velocity for Mode I and II cracks, and shear wave velocity for mode III cracks). The function $\beta(V_l/V_r)$ assumes values from unity to infinity as the ratio V_l/V_r varies from zero to unity [e.g., *Andrews*, 1976; *Freund*, 1998, p. 234]. The size of the dynamic process zone is given by $\Delta_T^d = \Delta_T/\beta$, where Δ_T is the equilibrium process zone length for a quasi-static crack (equation B4). The process zone becomes shorter as the rupture speed increases, up to vanishing when the limiting rupture velocity is approached ($V_r = V_l$) [*Ida*, 1972]. This is the LEFM limit, and the solution in Section 2.1.1 is retrieved.

Introducing an effective fracture energy as a work required to evolve the stress on a crack surface from σ_s to σ_d, $G_c = D_c(\sigma_s - \sigma_d)$, where D_c is the critical slip-weakening displacement at the base of the process zone ($\chi = L$), from equation (B6) one obtains

$$G_c = \frac{4a(1-\nu)}{\pi\mu}(\sigma_s - \sigma_d)^2 L \log\frac{1}{L} \tag{B8}$$

For a constant rupture velocity $V_r < V_l$, the assumption of a self-similar crack growth implies $L = const$. It follows that the fracture energy G_c, the slip-weakening displacement D_c, and the process zone length Δ_T are all assumed to linearly increase with the crack length.

Since the temperature increases due to faulting considered in Section 3 are non-dimensionalized using a characteristic strain drop ϵ, it is necessary to express ϵ in terms of the imposed boundary conditions and material properties for comparisons between different crack geometries and loading conditions. Making use of equations (B6)-(B7), one obtains

$$\epsilon = \frac{D(0)}{a} = \frac{4(1-\nu)}{\pi\mu}(\sigma_s - \sigma_d) L \log\frac{1+\sqrt{1-L^2}}{L}. \tag{B9}$$

For the LEFM crack ($L \to 1$), equations (B9) and (B4) reduce to

$$\epsilon = \frac{2(1-\nu)}{\mu}(\sigma_0 - \sigma_d). \tag{B10}$$

References

Abercrombie, R., Earthquake source scaling relationships from -1 to 5 M_L using seismograms recorded at 2.5-km depth, *J. Geophys. Res.*, *100*, 24,015–24,036, 1995.

Andrews, D. J., Rupture velocity of plane strain shear cracks, *J. Geophys. Res.*, *81*, 5679–5687, 1976.

Andrews, D. J., A fault constitutive relation accounting for thermal pressurization of pore fluid, *J. Geophys. Res.*, *107*, 10.1029/2002JB001,942, 2002.

Barenblatt, G. I., The formation of equilibrium cracks during brittle fracture, General ideas and hypotheses, Axially-symmetric cracks, *Appl. Math. Mech.*, *23*, 622–636, (in Russian), 1959.

Ben-Zion, Y., Properties of seismic fault zone waves and their utility for imaging low-velocity structures, *J. Geophys. Res.*, *103*, 12,567–12,585, 1998.

Ben-Zion, Y., and D. J. Andrews, Properties and implications of dymanic rupture along a material interface, *Bull. Seismol. Soc. Am.*, *88*, 1085–1094, 1998.

Beroza, G. C., and T. Mikumo, Short slip duration in dynamic rupture in the presence of heterogeneous fault properties, *J. Geophys. Res.*, *101*, 22,449–22,460, 1996.

Blanpied, M., T. Tullis, and J. Weeks, Effects of slip, slip rate, and shear heating on the friction of granite, *J. Geophys. Res.*, *103*, 489–511, 1998.

Bowden, F. B., and D. Tabor, *The Friction and Lubrication of Solids*, Clarendon Press, Oxford, 1954.

Broberg, K., Transient sliding motion, *Geophys. J. R. Astron. Soc.*, *52*, 397–432, 1978.

Brune, J. N., T. Henyey, and R. Roy, Heat flow, stress, and rate of slip along San Andreas fault, California, *J. Geophys. Res.*, *74*, 3821–4009, 1969.

Byerlee, J., Friction of rock, *Pure Appl. Geophys.*, *116*, 615–626, 1978.

Cardwell, R. K., D. S. Chinn, G. F. Moore, and D. L. Turcotte, Frictional heating on a fault zone with finite thickness, *Geophys. J. Roy. Astron.*, *52*, 525–530, 1978.

Carslaw, H. S., and J. C. Jaeger, *Conduction of Heat in Solids*, 510 pp., Oxford Univ. Press, New York, 1959.

Chester, F. M., and J. S. Chester, Ultracataclasite structure and friction processes of the Punchbowl fault, San Andreas system, California, *Tectonophysics*, *295*, 199–221, 1998.

Day, S. M., Three-dimensional simulation of spontaneous rupture: The effect of nonuniform prestress, *Bull. Seismol. Soc. Am.*, *72*, 1881–1902, 1982.

Dieterich, J. H., Earthquake nucleation on faults with rate- and state-dependent strength, *Tectonophysics*, *211*, 115–134, 1992.

Dugdale, D. S. J., Yielding of steel sheets containing slits, *Mech. Phys. Solids*, *8*, 100–115, 1960.

Fialko, Y., Time- and temperature-dependent evolution of stresses in a fault zone after the onset of frictional melting: Hints from numerical experiments, *Eos Trans. AGU Suppl.*, *80*, F682, 1999.

Fialko, Y., D. Sandwell, D. Agnew, M. Simons, P. Shearer, and B. Minster, Deformation on nearby faults induced by the 1999 Hector Mine earthquake, *Science*, *297*, 1858–1862, 2002.

Fialko, Y. A., and A. M. Rubin, Numerical simulation of high pressure rock tensile fracture experiments: Evidence of an increase in fracture energy with pressure?, *J. Geophys. Res.*, *102*, 5231–5242, 1997.

Fialko, Y. A., and A. M. Rubin, Thermodynamics of lateral dike propagation: Implications for crustal accretion at slow-spreading mid-ocean ridges, *J. Geophys. Res.*, *103*, 2501–2514, 1998.

Freund, L. B., The mechanics of dynamic shear-crack propagation, *J. Geophys. Res.*, *84*, 2199–2209, 1979.

Freund, L. B., *Dynamic fracture mechanics*, 563 pp., Cambridge Univ. Press, New York, 1998.

Goldsby, D., and T. Tullis, Low frictional strength of quartz rocks at subseismic slip rates, *Geophys. Res. Lett.*, *29*, art. no.–1844, 2002.

Guduru, P., A. Zehnder, A. Rosakis, and G. Ravichandran, Dynamic full field measurements of crack tip temperatures, *Eng. Frac. Mech.*, *68*, 1535–1556, 2001.

Heaton, T., Evidence for and implications of self-healing pulses of slip in earthquake rupture, *Phys. Earth Planet. Inter.*, *64*, 1–20, 1990.

Ida, Y., Cohesive force across the tip of a longitudinal-shear crack and Griffith's specific surface energy, *J. Geophys. Res.*, *77*, 3796–3805, 1972.

Ide, S., and M. Takeo, Determination of constitutive relations of fault slip based on seismic wave analysis, *J. Geophys. Res.*, *102*, 27,379–27,391, 1997.

Jeffreys, H., On the mechanics of faulting, *Geol. Mag.*, *79*, 291–295, 1942.

Kanamori, H., and D. L. Anderson, Theoretical basis of some empirical relations in seismology, *Bull. Seis. Soc. Amer.*, *65*, 1073–1095, 1975.

Kanamori, H., and T. H. Heaton, Microscopic and macroscopic physics of earthquakes, in *Physics of Earthquakes, Geophysical Monograph, 106*, edited by J. Rundle, D. L. Turcotte, and W. Klein, pp. 117–136, AGU, Washington, DC, 2000.

Khazan, Y. M., and Y. A. Fialko, Fracture criteria at the tip of fluid driven cracks in the Earth, *Geophys. Res. Lett.*, *22*, 2541–2544, 1995.

Lachenbruch, A. H., Frictional heating, fluid pressure, and the resistance to fault motion, *J. Geophys. Res.*, *85*, 6097–6112, 1980.

Lachenbruch, A. H., and J. H. Sass, Heat flow and energetics of the San Andreas fault zone, *J. Geophys. Res.*, *85*, 6185–6222, 1980.

Lawn, B., *Fracture of Brittle Solids - Second Edition*, 378 pp., Cambridge University Press, Cambridge, 1993.

Lee, T.-C., and P. Delaney, Frictional heating and pore pressure rise due to fault slip, *Geophys. J. R. Astron. Soc.*, *88*, 569–591, 1987.

Leonov, M. Y., and V. V. Panasyuk, The development of very small cracks in a solid, *Prikl. Mekh. (Applied Mechanics)*, *5*, 391–401, (in Ukrainian), 1959.

Levy, N., P. Marcal, W. Ostergre, and J. Rice, Small scale yielding near a crack in plane strain - Finite element analysis, *Int. J. Fract. Mech.*, *7*, 143–149, 1971.

Maddock, R., Frictional melting in landslide-generated frictionites (hyalomylonites) and fault-generated pseudotachylytes - discussion, *Tectonophysics*, *128*, 151–153, 1986.

Mair, K., and C. Marone, Shear heating in granular layers, *Pure Appl. Geophys.*, *157*, 1847–1866, 2000.

Manighetti, I., G. King, Y. Gaudemer, C. Scholz, and C. Doubre, Slip accumulation and lateral propagation of active normal faults in Afar, *J. Geophys. Res.*, *106*, 13,667–13,696, 2001.

Mase, C. W., and L. Smith, Effects of frictional heating on the thermal, hydrologic, and mechanical response of a fault, *J. Geophys. Res.*, *92*, 6249–6272, 1987.

McBirney, A., *Igneous petrology*, 2nd ed., 508 pp., Jones and Bartlett, Boston, 1993.

McGarr, A., Some constraints on levels of shear stress in the crust from observations and theory, *J. Geophys. Res.*, *85*, 6,231–6238, 1980.

McKenzie, D., and J. N. Brune, Melting on fault planes during large earthquakes, *Royal Astron. Soc. Geophys. Jour.*, *29*, 65–78, 1972.

Mora, P., and D. Place, Simulation of the frictional stick-slip instability, *Pure Appl. Geophys.*, *143*, 61–87, 1994.

Morse, P., and H. Feshbach, *Methods of theoretical physics*, 997 pp., McGraw-Hill, New York, 1953.

Olsen, K., R. Madariaga, and R. Archuleta, Three-dimensional dynamic simulation of the 1992 Landers earthquake, *Science*, *278*, 834–838, 1997.

Otsuki, K., N. Monzawa, and T. Nagase, Fluidization and melting of fault gouge during seismic slip: Identification in the Nojima fault zone and implications for focal earthquake mechanisms, *J. Geophys. Res.*, *108*, 10.1029/2001JB001,711, 2003.

Palmer, A. C., and J. R. Rice, The growth of slip surfaces in the progressive failure of over-consolidated clay, *Proc. R. Soc. London, Ser. A*, *332*, 527–548, 1973.

Perrin, G., J. R. Rice, and G. Zheng, Self-healing slip pulse on a frictional surface, *J. Mech. Phys. Solids*, *43*, 1461–1495, 1995.

Price, N. J., Laws of rock behaviour in the earth's crust, in *Rock mechanics - Theory and practice*, edited by W. H. Somerton, pp. 1–23, Am. Inst. Mining and Metall. Engineers Symposium on Rock Mechanics, 11th, Berkeley, Calif., 1970.

Rice, J., Flash heating at asperity contacts and rate-dependent friction, *Eos Trans. AGU Suppl.*, *80*, F682, 1999.

Rice, J. R., The mechanics of earthquake rupture, in *Physics of the Earth's Interior*, edited by A. M. Dziewonski and E. Boschi, pp. 555–649, North-Holland, Amsterdam, 1980.

Rice, J. R., and N. Levy, Local heating by plastic deformation at a crack tip, in *The physics of strength and plasticity*, edited by A. Argon, pp. 277–292, MIT Press, Cambridge, MA, 1969.

Richards, P., Dynamic motions near an earthquake fault - 3-dimensional solution, *Bull. Seism. Soc. Am.*, *66*, 1–32, 1976.

Rubin, A. M., Propagation of magma-filled cracks, *Annu. Rev. Earth Planet. Sci.*, *23*, 287–336, 1995.

Ruina, A., Slip instability and state variable friction laws, *J. Geophys. Res.*, *88*, 10,359–10,370, 1983.

Sammis, C., G. King, and R. Biegel, The kinematics of gouge deformation, *Pure Appl. Geophys.*, *125*, 777–812, 1987.

Scholz, C. H., *The mechanics of earthquakes and faulting*, 439 pp., Cambidge Univ. Press, New York, NY, 1990.

Scruggs, V., and T. Tullis, Correlation between velocity dependence of friction and strain localization in large displacement experiments on feldspar, muscovite and biotite gouge, *Tectonophysics*, *295*, 15–40, 1998.

Segall, P., and J. R. Rice, Dilatancy, compaction, and slip instability of a fluid infiltrated fault, *J. Geophys. Res.*, *100*, 22,155–22,171, 1995.

Sibson, R., Kinetic shear resistance, fluid pressures and radiation efficiency during seismic faulting, *Pure Appl. Geophys.*, *115*(1-2), 387–400, 1977.

Sibson, R., Power dissipation and stress levels on faults in the upper crust, *J. Geophys. Res.*, *85*, 6239–6247, 1980.

Sibson, R. H., Interaction between temperature and pore-fluid pressure during earthquake faulting - A mechanism for partial or total stress relief, *Nature*, *243*, 66–68, 1973.

Sibson, R. H., Generation of pseudotachylite by ancient seismic faulting, *Geophys. J. R. astr. Soc.*, *43*, 775–794, 1975.

Sleep, N., E. Richardson, and C. Marone, Physics of friction and strain rate localization in synthetic fault gouge, *J. Geophys. Res.*, *105*, 25,875–25,890, 2000.

Spray, J. G., Viscosity determinations of come frictionally generated silicate melts-Implications for fault zone rheology at high-strain rates, *J. Geophys. Res.*, *98*, 8053–8068, 1993.

Suppe, J., *Principles of structural geology*, 537pp., Prentice-Hall, Englewood Cliffs, NJ, 1985.

Swanson, M. P., Fault structure, wear mechanisms and rupture processes in pseudotachylyte generation, *Tectonophysics*, *204*, 223–242, 1992.

Teufel, L. W., and J. M. Logan, Effect of shortening rate on the real area of contact and temperature generated during frictional sliding, *Pure Appl. Geophys.*, *116*, 840–865, 1978.

Tse, S. T., and J. R. Rice, Crustal earthquake instability in relation to the depth variation of frictional slip properties, *J. Geophys. Res.*, *91*, 9452–9472, 1986.

Tsutsumi, A., and T. Shimamoto, High-velocity frictional properties of gabbro, *Geophys. Res. Lett.*, *24*, 699–702, 1997.

Turcotte, D. L., and G. Schubert, *Geodynamics, 2nd ed.*, 456 pp., Cambridge Univ., New York, NY, 2002.

Vidale, J., and Y. Li, Damage to the shallow Landers fault from the nearby Hector Mine earthquake, *Nature*, *421*, 524–526, 2003.

Wald, D. J., and T. H. Heaton, Spatial and temporal distribution of slip for the 1992 Landers, California, earthquake, *Bull. Seismol. Soc. Am.*, *84*, 668–691, 1994.

Wallace, R. C., Partial fusion along the Alpine Fault Zone, New Zealand, *Geological Society of America Bulletin*, *87*, 1225–1228, 1976.

Wenk, H.-R., L. Johnson, and L. Ratschbacher, Pseudotachylites in the Eastern Peninsular Ranges of California, *Tectonophysics*, *321*, 253–277, 2000.

Yoffe, E., The moving Griffith crack, *Philos. Mag.*, *42*, 739–750, 1951.

Zheng, G., and J. Rice, Conditions under which velocity-weakening friction allows a self-healing versus a cracklike mode of rupture, *Bull. Seism. Soc. Am.*, *88*, 1466–1483, 1998.

Y. Fialko, Institute of Geophysics and Planetary Physics, Scripps Institution of Oceanography, University of California San Diego, La Jolla, CA 92093. (e-mail: fialko@radar.ucsd.edu)

Table 1. Slip pulse characteristics of some earthquakes [*Heaton*, 1990], and the inferred lower bound on dynamic friction

Event, year	Magnitude	Rise time, s	D_{max}, m	σ_d, MPa
Michoacan, 1988	8.1	5.0	6.5	3.2
Borah Peak, 1983	7.3	0.6	1.47	5.0
San Fernando, 1971	6.5	0.8	2.5	3.4
Imperial Valley, 1979	6.5	1.0	1.8	5.3
Morgan Hill, 1984	6.2	0.3	1.0	5.2
Palm Springs, 1986	6.0	0.4	0.45	13.4
Coyote Lake, 1979	5.9	0.5	1.2	5.6

Assumed thermophysical parameters: ΔT=500 K; thermal diffusivity κ=10^{-6} m^2/s; heat capacity c=10^3 J/kg; rock density ρ=2.7×10^3 kg/m^3